Heritage Science

RESEARCH

Open Access

Appearance-based evaluation of varnish removal methods in gilded surfaces

Yoko Arteaga[1,2*], Diane Marchioni[3], Stéphanie Courtier[1], Clotilde Boust[1,4] and Jon Y. Hardeberg[2]

Abstract

This paper outlines the use of bidirectional reflectance measurements for the characterisation and evaluation of appearance changes in gilded surfaces caused by varnishing and cleaning. Oil and water gilding mock-ups representative of a 15th-century panel painting were varnished, and a selection of four varnish removal methods was applied. By measuring the bidirectional reflectance of the samples, their appearance was modelled and evaluated according to perceptual gloss attributes. Three main perceptual groups were found for each gilding type: unvarnished, varnished and cleaned surfaces. Finally, for the studied samples, the most appropriate method for removing dammar and colophony varnish from a gilded surface, in terms of appearance change, is solubilisation by applying an Evolon®CR compress.

Keywords Gilding, Material appearance, BRDF measurement, Varnish removal, Gloss

Introduction

Gilding is a form of polychromy where a gold leaf is attached to a substrate by different means. Commonly used in the Middle Ages, gilding gives a golden appearance to a surface dependent on its fabrication method. While oil gilding is believed to have a cooler appearance due to its matte and rough surface, water gilding is described as warmer and glossier due to burnishing which smooths the surface and gives it a metallic appearance [1].

It is common to find gilded surfaces that have been varnished for various reasons: to protect the surface from abrasions and mechanical damages [2, 3], to change its appearance [4], and to imitate another metal [5, 6]. Varnish can change the appearance of a gilded surface by modulating its gloss, or depending on the varnish, change its hue [3].

However, varnish is an organic material which changes appearance over time. Common restoration techniques involve cleaning the superficial layer, leaving the varnish intact, or removing the varnish without damaging the surface underneath it. Due to the fragility of the gold leaf, it is important to understand the mechanisms at play when removing the varnish to avoid any damage or modification to the gilded surface. Empirical knowledge on the appearance of gilding is vast amongst conservators and restorers; appearance differences between distinct types of gilding as well as conservation treatment effects such as varnishing are well understood in this community. However, these appearance changes have not been thoroughly studied in a quantifiable manner which correlates to perception.

Gilded surfaces have a metallic appearance which cannot be described solely with traditional colorimetry since many elements influence how it is perceived. While the appearance of diffuse materials such as mineral pigments can be described by colour measurements, the appearance of metallic surfaces is mainly described by their colour and gloss [7]. Materials which present colour changes

*Correspondence:
Yoko Arteaga
yoko.arteaga@culture.gouv.fr
[1] Centre of Research and Restoration of the Museums of France, Paris, France
[2] Department of Computer Science, Norwegian University of Science and Technology, Gjøvik, Norway
[3] National Heritage Institute, Paris, France
[4] PSL-PCMTH UMR8247, CNRS, Paris, France

under different illumination-viewing conditions, such as gilding, are called goniochromatic [8]. Three viewing geometries have been defined suitable to describe metallic paints: near-specular, face, and flop angles [9]. Vast research has been done to characterise goniochromatic films and paints [10, 11]. However, this has not been applied to gilding.

In the case of gilding, colour differences calculated for a fixed angle of incidence and reflection may be unrepresentative of perceptual differences. Gloss measurements provide angular information, as they are performed at three different angles; and thus, its perception is highly dependent on illumination and viewing directions. However, the correlation between gloss units and human perception is not clearly defined [12]. It is found gloss perception has a nonlinear relationship with instrumental gloss values and many factors such as binocular vision influence gloss sensitivity [13]. Recommendations by experts and industry are to perform psychophysical experiments to define gloss tolerances for a batch of samples [14]. In the case of gilded surfaces, many factors can affect their visual perception such as the illumination type, geometry and intensity, the viewing conditions, the material composition of the gilding, and the presence of surface coatings, to name a few [15].

For many applications, complex surface appearance can be characterised by the bidirectional reflectance distribution function (BRDF) which is the physical quantity for gloss measurement [16]. The BRDF describes how light is reflected off a surface and depends on illumination and viewing directions. Multidirectional reflectometry is an approach in which one directly measures the ratio of reflected over incident light at each combination of angles to model the BRDF of a given surface. This method allows obtaining a full model of the BRDF which can describe the appearance of the surface at different combinations of viewing and illumination directions.

It is thus, of great interest to measure the BRDF of gilded surfaces to characterise their appearance. By obtaining a more accurate appearance measurement, the effect that conservation treatments such as varnishing, and its eventual removal, have on the perception of gilded surfaces can be evaluated. Varnish is believed to increase the saturation of colours and the gloss of surfaces, altering the appearance and perception of the artwork. While this is well documented in the case of pigments, its effect on gilding has not been studied. Finally, varnish removal methods can be evaluated to find which will, amongst other desirable qualities, return the gilded object the closest to its original appearance.

This work has been developed in conjunction with the National Heritage Institute in Paris, France, as part of a final-year conservation studies project dedicated to a 15-th century framed panel painting, named after its iconography, the *Vierge de douleur/Virgin of Sorrows* and belonging to the Jacquemart-André Museum in Paris. (Fig. 1).

The technological study of the artwork revealed that the gilding present on the *Vierge de douleur/Virgin of sorrows* was covered with a thick layer of coloured varnish. The analysis showed that this layer was constituted of different types of varnish, including an original varnish which constituted the original decor of the painting. Therefore, the aim of removing the varnish by using chemical methods is not to completely remove the varnish from the gilded surface but to remove superficial layers of the soiled varnish by controlling the surface appearance. In addition, the adhesive of the gold leaf on the original gilding could have been soluble in the same solvents as the varnish, demanding a very controlled protocol. The main results of the technological study of the painted panel are presented in the Appendix.

Research aims

The primary aim of this paper is to propose a framework to measure, quantify, and evaluate the appearance of gilded surfaces. The second aim is to apply the presented framework to evaluate appearance changes induced by different chemical varnish removal methods on varnished, gilded wood. Finally, these findings can be used to potentially guide the restoration of the painting. An imaging-based method is presented to measure the BRDF of two types of gilding mock-ups. These have been varnished and four chemical varnish removal methods have been tested. The BRDF of the surface is modelled and the BRDF parameters are used to classify the gilding in terms of its appearance.

Fig. 1 Unknown. *Vierge de douleur/Virgin of sorrows*. 15th century. Painted panel. 36.8 x 34.0 cm (62.3 x 43.0 cm with frame). Jacquemart-André Museum, Paris. **a** Before restoration. **b** After restoration. ©Angèle Dequier/Inp

Background

Gilding fabrication techniques

The samples designed for this study are intended to be representative of the gilding present on the studied artwork. Thus, the findings can potentially be used directly for restoration. Two types of gilding were produced, water gilding, representative of the frame, and oil gilding. Although the gilding of the painted panel was not identified with certainty when the samples were produced, it seemed more likely that it was oil gilding. Even if this is ultimately not the case, it is still valuable to compare the behaviour of these two types of gilding when faced with cleaning. Indeed, these are the two major traditional gilding techniques [17], the use of which has moreover changed very little since the Middle Ages.

The difference between oil gilding and water gilding lies mainly in the nature of the mordant, i.e., the layer underlying the gold leaf (Fig. 2). In the first case, the mordant is an oil-based mixture. It is laid on a thin sealer layer of shellac which has an insulating and saturating function. In the second case, it is a bole, a preparation based on clay or natural soil. This layer is placed on a yellow size which can be made of different preparations and creates a mechanical grip for the next layer and provides a first coloured shade under the gilding.

In the case of oil gilding, the mordant with oil must be left to partially dry. When it is tacky, it is ready to receive the gold leaf, which adheres immediately. Regarding water gilding, the bole is moistened with water; the gold leaf adheres to it immediately. After drying, the gold leaf can be burnished, that is, smoothed on the bole with a hard tool like an agate stone, to make it shiny and smooth. Unlike water gilding, the gold leaf in oil gilding cannot be burnished, so it remains matte and relatively rough.

Removal of varnish in gilded surfaces

Removal of varnish is a widely studied and documented restoration intervention, particularly in the field of painting restoration. In recent decades, this field has benefited from the contribution of substantial scientific research [18–20] which has made it possible to better understand the mechanisms of solubilisation of organic films, and to introduce new cleaning methods. These always aim to find the best compromise between cleaning efficiency and harmlessness in relation to the artwork. However, unlike mechanical cleaning [21, 22], chemical cleaning methods have not been vastly studied on a gilded wood substrate. The study closest to this subject concerns the chemical removal of a brass-based overpaint on gilded wood [23] and cleaning soiled gilded wood [24]. Another study deals with the chemical cleaning of a brass object [25]. A survey of restorers specialising in this field reveals a relatively empirical practice, for lack of publications on the subject.

The Getty Conservation Institute devoted a study day [26] to the problem of cleaning gilded wood. The report describes the methods used by gilding conservators as well as the specific constraints of gilding on wood. Gilding is a surface treatment with a complex stratigraphy (Fig. 2). It is widely present on heritage objects and can exist on substrates other than wood. There are great differences between gilding on varied substrates, each requiring a different surface preparation and a different restoration approach. It is therefore essential to better understand its behaviour to adapt restoration practices accordingly. The authors of the report raise three problems induced by cleaning: the persistence of cleaning residues (especially in the case of gels), the penetration of solvents under the gold leaf (which can then partially solubilise or alter the substrate), and finally weathering of the gold leaf. The persistence of residues is a phenomenon studied in the field of painted surfaces [27]; its consequences, whatever the nature of the surface, seem to be the same: the residues can cause irreversible damage to the artwork, modify the surface appearance, and are quick to clog up or retain moisture.

Gold leaf, which is extremely thin (0.1 to 10 μm), is fragile [28] and can be altered in different ways: by mechanical abrasion, i.e. the loss of material during cleaning, and by modifying the surface appearance, in particular its gloss and colour. Cleaning is, in its general definition, the removal of all secondary debris and soiling which distract the perception and interpretation of the original surface. The secondary debris and soling can sometimes form a film if deposited in the form of a layer, but they can be also be found in the form of uneven accretions on the surface. For the sake of clarity, this study refers to the removal of varnish, even though it is desirable that a thin layer of varnish is left on the surface. This paper focuses on the alteration of the surface appearance of gilding caused by varnishing and its subsequent removal.

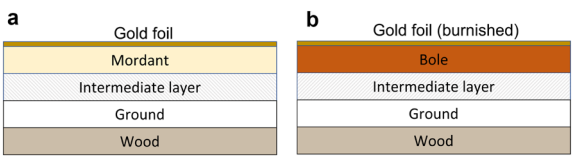

Fig. 2 General stratigraphy of (**a**) oil gilding and (**b**) water gilding. In the case of water gilding, the gold foil is burnished

Appearance measurement of gilded surfaces

Gilded surfaces present very interesting appearance properties. While the appearance of diffuse and opaque surfaces such as mineral pigments can easily be described by their colour, specular surfaces such as gilding require complex BRDF measurements in order to correlate them with their perceived appearance. These appearance measurements provide macroscopic characteristics, represented as a statistical aggregation of the reflection of light from many microfacets on the materials surface. Gilded or golden surfaces in cultural heritage objects pose technical imaging challenges.

In order to evaluate the influence of lighting conditions on spectral reconstruction and image stitching using multispectral images, a traditional Japanese painting was imaged with a multispectral camera [29]. The spectra were well estimated for the regions with an orange mineral pigment. However, the gilded region which exhibited high specular reflection presented a poor spectral reconstruction. None of the lighting configurations provided an accurate reconstruction of the reflectance spectrum. The lighting parameters were not optimised for this object and the authors conclude that to achieve better spectral reconstruction, specular reflection issues must be solved.

In the assessment of multispectral and hyperspectral imaging systems, a Round Robin Test assessed the performance of different systems for their spectral digitisation of artworks [30]. The artwork chosen was a polychrome Russian icon from the 19th century, fabricated in Moscow. The icon depicts the subject of the Virgin of Kazan and is printed in chromolithography onto a substrate of tinned steel. This icon was chosen because of its physical and material characteristics. It has a medium gloss on the painted areas and the gold areas have a shiny metallic finish. In the case of the gold area, the authors found significant differences in the reflectance spectra. The shape of the spectra was the same for all imaging systems, however the difference in magnitude varied by a factor of as much as 3x either higher or lower than the reference measurement. This was attributed to the granular nature of the surface and the breadth of the specular peak, characteristic to golden surfaces, which caused the image intensity to be critically dependent on its illumination geometry. The authors conclude that the imaging geometry plays a vital role on glossy surfaces, and it is essential to have some flexibility in the position of the light source and object relative to the camera so the operator can modify the setup according to judgement.

According to the recommendations given in [30], a multi-focus high-dynamic range (HDR) visible/near-infrared (VIS/NIR) hyperspectral imaging set-up is presented for its application to works of art [31]. In this work, the authors present a complete framework for capturing and processing hyperspectral images of works of art in situ. This framework is applied to a facsimile of *The Golden Haggadah* from the British Library of London which presents gilded areas with high specular reflection. The authors propose a framework in which an HDR hyperspectral image is obtained. Although the final HDR image of the manuscript did not necessarily contain HDR information, the HDR was present in radiances where powerful light sources or dim shadowy areas are present in the same scene which is the case of paintings with gilded areas. The authors segmented gilded from non-gilded areas in the image, based on the spectral reflectance, and compared it to manual segmentation performed by a conservator. The HDR cube had a much better segmentation performance of 95.5% compared to that of the low-dynamic range (LDR) cube of 83.78%. Moreover, while the LDR cube was saturated in some golden areas, the HDR cube was correctly exposed throughout the scene.

In the case of measuring the appearance of gilded surfaces, the most common method is colorimetry. Dumazet et al. [32] used Kubelka-Munk's two flux theory to model the influence of the substrate's colour on the reflected light from the gold leaf, in order to study correlations between gold leaf's imperfections and appearance. The authors made oil gilding mock-ups on stone and measured the back-scattered light at normal incidence of the samples. They have found a red shift in the spectrum when the concentration of holes is higher. Mounier et al. [33] also present colorimetric observations on the appearance of gold leaf on white, red, and black substrates. Oil and distemper gilding mock-ups representative of mural paintings were fabricated and artificially aged. The transmission spectra of different thicknesses of gold leaf were measured and the CIE L*a*b* coordinates were compared individually.

Wu et al. [15] study the influence of substrate colour on the visual appearance of gilding. Gilding mock-ups were fabricated using different methods such as oil gilding, water gilding, and ground gilding. The authors used colorimetry and interferometric microscopy to characterise the mock-ups and conclude that the colour of the substrate does not alter the visual appearance of the gilding. However, they report that burnishing the gilding produces a significant change in appearance.

Finally, Sandu et al. [3] study the surface behaviour of water gilding and imitation gilding using liquid gold. The mock-ups were analysed before and after burnishing (for the water gilded samples), and varnishing. The authors have measured the mock-ups' colour in a

diffuse geometry of 0/0. They report that the CIE L* value decreases after burnishing and imply a decrease in lightness which contradicts the hypothesis that burnishing increases gloss. The authors contribute these discrepancies to a poor burnishing and/or a different behaviour from the gold leaf imitation. While this may be true, it must be stressed that colorimetry measurements in a diffuse domain are not adequate for evaluating gloss. They also report that varnishing the surfaces, increases the L* value of the water gilded samples but decreases it in the case of liquid gold.

Bidirectional reflectance of polychrome wood composed of a silver leaf and yellow pine resin which gives it a golden appearance was measured using a spectroradiometer to detect changes in appearance due to accelerated ageing [34]. The authors measured small colour changes due to ageing but significant gloss changes and more specifically a shift in the specular peak. The unaltered samples looked considerably glossier than the aged samples. The goniometric measurements showed that the reflectance peaks which originally were symmetrical, become asymmetrical as an effect of ageing.

Bidirectional reflectance measurements of gold leaves used for gilding are performed in an attempt to model their BRDF [35]. A multi-angle spectrophotometer was used to measure the reflectance of the samples at 12 different combinations of incidence and observation directions. The authors find that the colour change of the gold leaves at different angles of incidence and reflection is significant. Moreover, they conclude it is necessary to properly sample measurement angles close to the specular peak to obtain accurate BRDF models.

The literature review shows there is a lack of research in appearance capturing of gilded surfaces. Multispectral and hyperspectral imaging systems are presented to digitise and capture objects where there are gilded or golden areas present on the scene [29–31]. The three authors emphasise the necessity of appropriate illumination and viewing directions for accurate image capture. However, the focus is on the imaging device's advantages and limitations, as well as the spatial and spectral quality of the data, not the appearance of the gilding. In the case of evaluating the appearance of gilded surfaces more specifically [3, 15, 32, 33], studies are limited to colorimetric measurements which are not sufficient to describe the complete visual appearance of gilding. Moreover, these do not evaluate the effect of removing varnish from gilded surfaces. Thus, it is necessary to measure the appearance of gilded surfaces accounting for viewing and illumination directions to provide a more complete evaluation [34, 35].

Materials and methods

Fabrication of gilding mock-ups

The gilding studied in this paper are common types of gilding found in the Middle Ages [17]. Water and oil gilding mock-ups were made by professional restorers using traditional techniques. The gold foil used for the gilding mock-ups is 22 karat *or Versailles* from Dauvet goldbeaters.

Four sets of mock-ups are produced using a plywood base. Two reference mock-ups with dimensions 11 x 6 cm, which are not varnished, and two test mock-ups with dimensions 22 x 11 cm (Fig. 3). The test mock-ups are varnished and then cleaned following the four methods described below. As part of the original investigation, two different varnishes were studied. However, in this paper, only one varnish is analysed. The preparation of each mock-up is detailed in Table 1.

The mock-ups are fabricated following traditional gilding techniques, with the same ground layer based on a chalk ground bound with diluted rabbit skin glue. In the case of oil gilding, an intermediate layer of shellac is applied on the ground and then, an oil-based gold size called mordant is used as substrate and adhesive. When the surface is tacky but not completely dry, the gold leaf is applied. For water gilding, an intermediate layer of rabbit skin glue and yellow ochre is applied, followed by a red bole. A mixture of ethanol and water is used as a wetting agent before applying the gold leaf. The gold leaf is burnished manually using an agate burnishing tool which is applied in one direction to produce a highly metallic gloss.

For each gilding technique, one reference sample is kept unvarnished. The test samples are varnished with a combination of dammar and colophony resins in equal proportions. This varnish was found on the artwork as part of past conservation work (see Appendix). To avoid any premature damage to the gold leaf, the varnish is sprayed on the mock-ups using an Ecospray® at 10 cm. Each surface is varnished five consecutive times. To accelerate the polymerisation of the resin, the mock-ups are placed inside a Suntest XLS / XSL + UV chamber, with 840780 kJm^{-2} power and energy flux of 765 Wm^{-2} for 311 h, at 35° C. The polymerisation of the resin impacts the adhesion and ductility of the materials as well as the cohesion of the stratigraphy. It aims to replicate as close as possible a real, aged, varnished, gilded surface, since these properties could influence the solubility of the varnish.

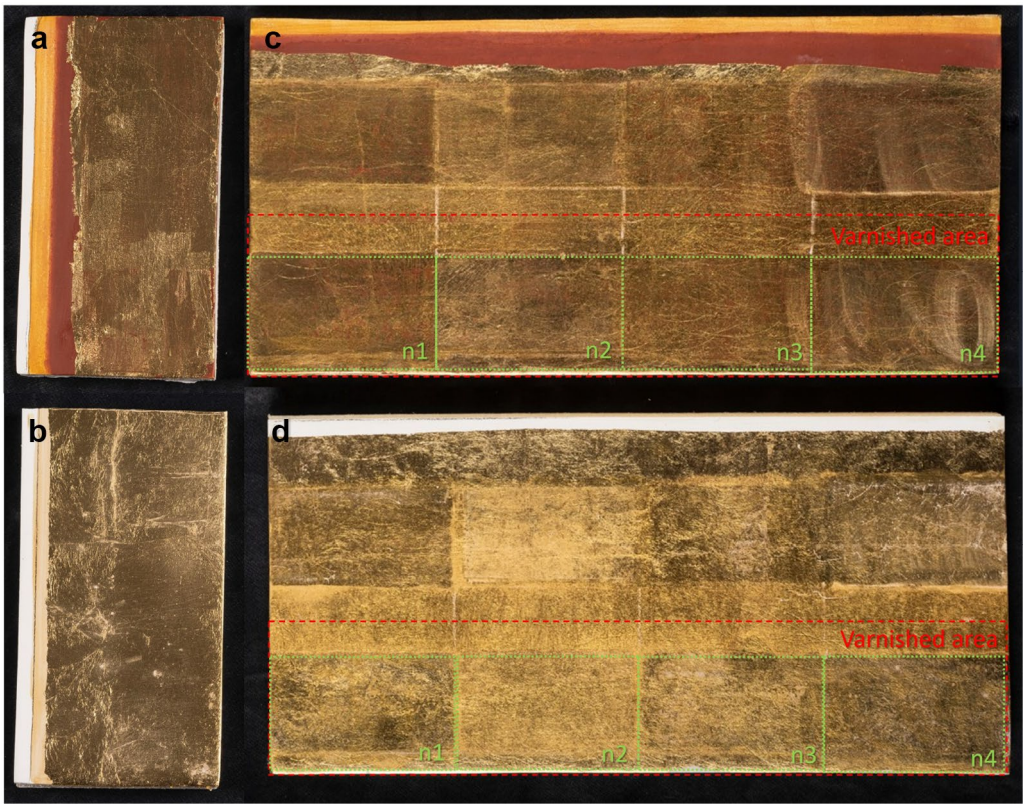

Fig. 3 Picture of the mock-ups fabricated. **a** Reference unvarnished water gilding. **b** Reference unvarnished oil gilding. **c** Varnished and cleaned water gilding. **d** Varnished and cleaned oil gilding. The red rectangle shows the varnished area with dammar and colophony. The green rectangles show the cleaned area for each method. ©Angèle Dequier/Inp

Varnish removal methods

Four chemical methods are tested to remove the varnish from the mock-ups. The methods chosen are commonly used in domains of conservation and restoration. The main principle is to use a solvent mixture of isooctane and ethanol in a 70:30 ratio [36], in four different ways. The varnish removal methods and their advantages and disadvantages are described below (Fig. 4).

Method 1: Solubilisation with a cotton swab (n1) This method is traditionally used when removing an organic film in paintings. The cotton swab is dipped in the mixture of solvents and applied on the surface with no pressure. When the cotton is saturated with varnish, a new cotton swab is used. The advantages of this method are the good control of the solubilisation action and the absence of residue on the surface. On the other hand, cotton is an abrasive material which can damage sensitive substrates since there is little control over the diffusion into the substrate and the evaporation of the solvent.

Method 2: Solubilisation by applying a compress (n2) This technique is widely used in the restoration and conservation of artworks. A compress of the same dimensions as the desired area to clean is placed on the surface and soaked with the solvent. The compress used here is an Evolon®CR textile due to its absorbing qualities, simple use, and satisfying results [37, 38]. A Melinex® plastic film is placed over the compress to avoid evaporation and a piece of glass is placed on top

Table 1 Structure and material composition of the mock-ups

Sample name	Type of gilding	Varnish	Type of cleaning
OG	Oil	No	N/A
OG-V	Oil	Yes	N/A
OG-V-n1	Oil	Removed	Method 1
OG-V-n2	Oil	Removed	Method 2
OG-V-n3	Oil	Removed	Method 3
OG-V-n4	Oil	Removed	Method 4
WG	Water	No	N/A
WG-V	Water	Yes	N/A
WG-V-n1	Water	Removed	Method 1
WG-V-n2	Water	Removed	Method 2
WG-V-n3	Water	Removed	Method 3
WG-V-n4	Water	Removed	Method 4

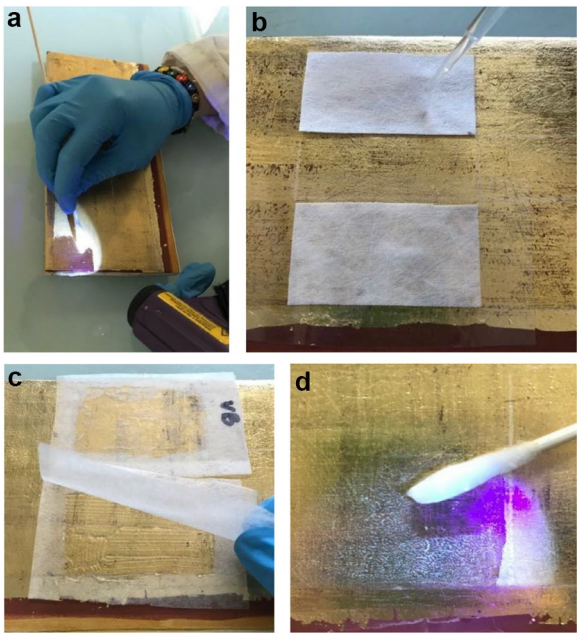

Fig. 4 Cleaning methods. **a** Solubilisation with a cotton swab under UV light. **b** Solubilisation by applying a compress. A pipette is used to soak the compress with the solvent. **c** Solubilisation by use of a gel. The gel is between two layers of hemp paper. **d** Rinsing the surface using a cotton swab

to apply pressure on the surface. The advantages of this method are that it does not require rubbing the surface, it does not leave fibrous residues, and it is an isotropic and resistant material [39]. However, there is little visual control over its action on the varnish and it can only be used on flat surfaces.

Method 3: Solubilisation by use of an aqueous gel (n3) A solvent gel is fabricated following the technique developed by Richard Wolbers [19]. The gelling agent is a polyacrylic acid, a long-chain synthetic polymer (Carbopol® type), which is neutralised by an organic base from the amine family with surfactant properties (Ethomeen® type). A hemp paper interface is used to manipulate the gel and avoid unnecessary rinsing and rubbing. After two minutes the gel is removed, and the surface is rinsed with isooctane using a cotton swab. The advantage of using a gel is that there is little penetration of solvents compared to free-handed methods like n1. Moreover, it can be applied to a specifically defined area and requires little rubbing as this is only necessary in the final rinsing stage. Nonetheless, the water content in the gel might alter water-sensitive surfaces such as oil gilding.

Method 4: Solubilisation by use of a silicon-based gel (n4) This method is applied in the same way as n3 but the gel chosen is silicon-based. The gel used here is a Shin Etsu KSG-350Z®. It can be coupled with silicone solvents with different molecular weights, called cyclomethicones. These are apolar solvents whose surface tension is very low. Their immiscibility with water, as well as their slow evaporation time, allow them to be used as a temporary "pore filler"; and thus, protect the substrate from the migration of other solvents. These evaporate more or less rapidly. The advantage of this method is that due to the silicon nature of the solvent, the substrate is temporarily protected. Also, this method is favourable for water-sensitive surfaces, and due to its high viscosity, the penetration of the solvent into the substrate is limited.

Conventional colour and gloss measurements

Colour measurements were carried out with a Konica Minolta CM-2600d spectrocolorimeter, at specular component excluded (SCE) mode to have only the diffuse light. 20 measurements were taken for each area, moving the device a few millimetres each time. Gloss measurements were taken with a Rhopoint Instruments Novo-Gloss glossmeter. The glossmeter measures at three angles of reflection (20°, 60°, and 85°). The measured area is 6.4 x 6 mm at 20°, 6 x 12 mm at 60°, and 4.4 x 4.4 mm at 85°. Since the measurement area is rather large, only three successive measurements at the same place were carried out, and the values were averaged in order to ensure their reproducibility. Both measurement systems are designed for flat surfaces. In the case of curved surfaces present in real objects, a different choice of noncontact device would be necessary.

Flexible HDR multispectral-imaging BRDF system

As previously explained in *Appearance measurement of gilded surfaces*, conventional colour and gloss measurements are insufficient to fully characterise the appearance of gilding. Thus, in this subsection, an alternative bidirectional reflectance acquisition and processing pipeline are presented.

The imaging system used in this paper has been described in [40]. It is composed of a five-joint robotic arm which holds the illumination source, a multispectral snapshot camera, and a tilted stage with an angle of elevation of 22.5° (Fig. 5). The multispectral camera captures eight narrow bands centred at 440 nm, 473 nm, 511 nm, 549 nm, 585 nm, 623 nm, 665 nm, and 703 nm. The camera is positioned vertically over the sample at 30 cm. The images are acquired at maximum zoom of 3x and maximum aperture size. The effective pixel size is 0.0377 mm. The robotic arm is capable of moving in a 70 ° arch on the y-z plane. Thus, the sample is tilted so it is illuminated at a fixed angle of observation, $\theta_r = -22.5°$, and the illumination angles cover an arch of 35° from both sides of the mirror angle, ranging from $\theta_i = -57.5°$ to $\theta_i = 12.5°$, with a total of 63 angles.

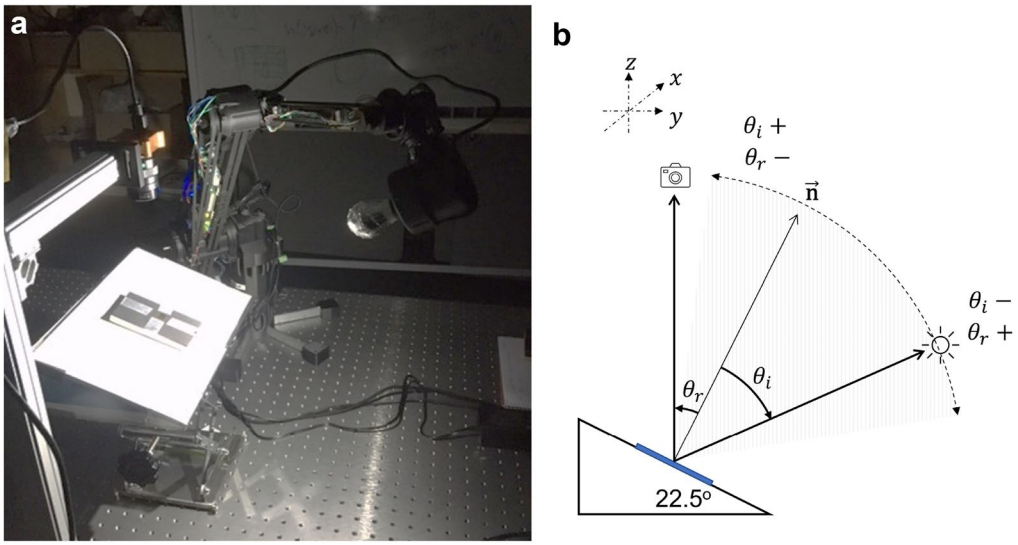

Fig. 5 Side view of the imaging system. The sample is placed on a tilted stage, the camera is above the sample and the light is held by a robotic arm. **a** Picture of the imaging system. **b** Schematic of the imaging system. (Robotic arm not illustrated). Taken from [40]

HDR acquisition pipeline

Due to the specularity of the samples and as suggested in [31], an HDR acquisition pipeline is developed. For each angle of illumination, ten images are taken at exposure times 1 ms, 2 ms, 4 ms, 8 ms, 16 ms, 32 ms, 64 ms, 125 ms, 250 ms, and 499 ms. Thus, for 63 angles of illumination, a total of 630 images are taken with an average time of 30 min per sample.

For each acquisition, a dark-current set of images is obtained at the same exposure times. The non-uniformity of the light source is corrected by performing a flat-field correction. This is done by acquiring a set of images of a uniform white reference target [41]. To perform the spectral reconstruction, a 30-patch ColorGauge Nano Target colour chart [42] which was measured using the HySpex VNIR-1800 hyperspectral imaging system at 45/0 measurement geometry, is also acquired using the imaging system. The reflectance factors are interpolated to the range 400 nm - 700 nm in steps of 10 nm in order to calculate a transformation matrix for each angle of illumination.The colour chart is made of a diffuse material so it is assumed that the reflectance spectra of the patches will not change significantly at different illumination directions.

Data processing pipeline

The data is processed to obtain an HDR BRDF of the sample, and has been described in [40] (Fig. 6). The HDR multispectral image is created following the method proposed by Brauers, et al. [43].

For each sample, at each angle of illumination, ten raw images with 10-bit depth are taken with different exposure times. The dark current is subtracted for each exposure time. Each image is linearised using a look-up-table,

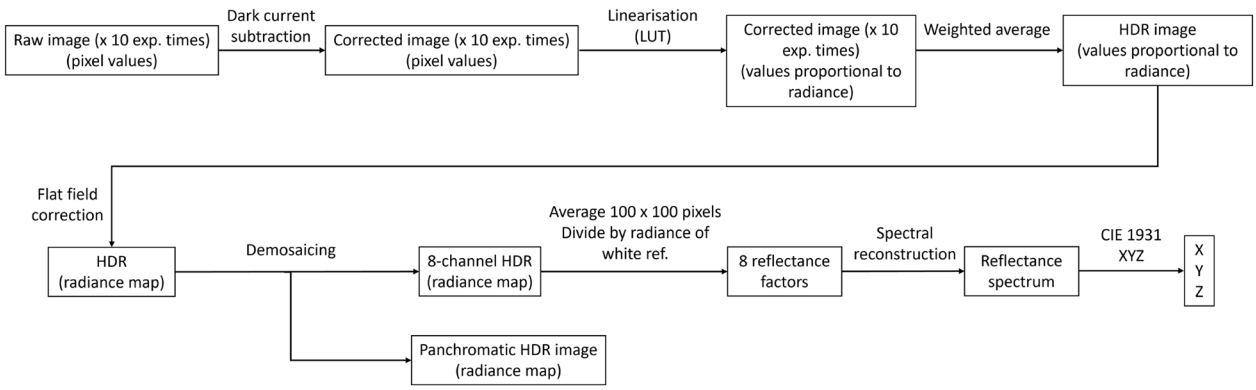

Fig. 6 Processing pipeline to obtain HDR BRDF of the samples as described in [40]

to obtain values proportional to the object's radiance. At this stage, the HDR image is created by performing a weighted average across exposure times using a modified Tukey window. A flat-field HDR image of a uniform nearly-Lambertian reference white calibration surface is generated following the same steps to correct for non-uniformity in the illumination. The flat-field correction is performed by multiplying the flat-field image with the HDR image. The HDR radiance map is demosaiced using bilinear interpolation where a multispectral image of 8 bands is obtained and a panchromatic image as the ninth channel.

An area of 100 x 100 pixels is averaged to obtain the discrete reflectance factors, $\mathbf{Q}$, at each spectral band. The spectral radiant power incident on the camera sensor is given by:

$$\phi = k\mathbf{HS}\beta. \tag{1}$$

$k = Aa$ is a camera specific factor, where A is the area of the sensor and a is the aperture of the optics. $\mathbf{H}$ are the spectral characteristics of the sensor filter array, $\mathbf{S}$ is the light source spectral irradiance, and β is the spectral reflectance.

Since H cannot be inverted, Equation 1 is re-arranged:

$$\phi = k\mathbf{S}'\mathbf{H}\beta. \tag{2}$$

By using the camera response values from the uniform nearly-Lambertian reference white calibration surface, ϕ_{ref}, the discrete spectrum of the light source, $\mathbf{S}_{\text{ref}}$, is approximated, where the reflectance spectrum of the white balance card, β_{ref}, is assumed to be that of a Lambertian surface.

Dividing $\phi \div \phi_{\text{ref}}$ is the equivalent of a multispectral white balance, cancelling out the specific camera factor k, and giving the discrete reflectance factors for each spectral band $\mathbf{Q}$:

$$\mathbf{Q} = \mathbf{H}\beta. \tag{3}$$

Given that $\mathbf{H}$ cannot be inverted, a transformation matrix, $\mathbf{T}$, is calculated using the known reflectance spectra, β_{cc}, and reflectance factors, $\mathbf{Q}_{\text{cc}}$, of the reference colour chart:

$$\mathbf{T} = \beta_{\text{cc}}\mathbf{Q}'_{\text{cc}}\text{inv}(\mathbf{Q}_{\text{cc}}\mathbf{Q}'_{\text{cc}} + \lambda\mathbf{I}), \tag{4}$$

where $\mathbf{I}$ is an identity matrix and $\lambda = 0.0003$ is a regularisation factor which avoids overfitting and guarantees smooth curves.

Thus, the reflectance spectrum, β_{est}, can be estimated using the following equation:

$$\beta_{\text{est}} = \mathbf{TQ}. \tag{5}$$

Bidirectional reflectance modelling

The bidirectional reflectance of the material is modelled using the BRDF defined by Nicodemus [44] as the ratio between the differential irradiance, E, along $\mathbf{l}$ at point x and the differential outgoing radiance, L, along $\mathbf{v}$:

$$f(x, \mathbf{l}, \mathbf{v}) = \frac{dL_r(x, \mathbf{v})}{dE(x, \mathbf{l})}. \tag{6}$$

Cook-Torrance BRDF

Cook and Torrance describe a physically based BRDF model based on geometrical optics [45]. This model is a well-established physical model and is used extensively to model specular materials like gold [35, 45–47]. The BRDF is separated into a specular, R_s, and a diffuse, R_d component:

$$f = k_d R_d + k_s R_s, \tag{7}$$

where k_d and k_s are weighting parameters and $k_d + k_s = 1$. The specular term is based on micro-facet theory, which dictates that only the micro-facets on the surface with orientations in between the viewing vector and the incident vector, called half-vector, $\mathbf{h} = \mathbf{l}.\mathbf{v}$, will contribute to the reflected light.

The general form of the Cook-Torrance specular term is:

$$R_s = \frac{1}{\pi}\frac{FDG}{(\mathbf{n}.\mathbf{l})(\mathbf{n}.\mathbf{v})}, \tag{8}$$

where F is the Fresnel term [48], G is the geometrical attenuation factor accounting for shadowing and masking of micro-facets, D is the distribution of normals facing $\mathbf{h}$, and $\mathbf{n}$ is the surface normal.

In this paper a simplified isotropic Cook-Torrance BRDF model is used:

$$I_p = \begin{bmatrix} I_{Px} \\ I_{Py} \\ I_{Pz} \end{bmatrix} = I_a R_a + I_i \cos\theta_i \left(k_s R_s + (1 - k_s) \begin{bmatrix} R_{dx} \\ R_{dy} \\ R_{dz} \end{bmatrix} \right), \tag{9}$$

where I_p is the CIE tristimulus value at point P with incident angle θ_i and at fixed reflection angle $\theta_r = -22.5°$. $I_a R_a$ is the ambient light term which is assumed to be zero as the experiment is performed in a dark environment. I_i is the incident light intensity, R_d are the spectral diffuse reflectance components. The specular components, R_s, are given by the Cook-Torrance GGX specular term (Eq. 15). (For more details on BRDF models refer to the Appendix.)

For each measurement, the CIE XYZ tristimulus values are calculated using the reflectance spectra, $S(\lambda)$, D65 illuminant, $I(\lambda)$, and CIE 1931 colour matching functions, $\bar{x}(\lambda)$, $\bar{y}(\lambda)$, and $\bar{z}(\lambda)$, according to:

$$\begin{bmatrix} X \\ Y \\ Z \end{bmatrix} = \frac{1}{N} \int_{\lambda} S(\lambda) I(\lambda) \begin{bmatrix} \bar{x}(\lambda) \\ \bar{y}(\lambda) \\ \bar{z}(\lambda) \end{bmatrix} d\lambda, \tag{10}$$

where

$$N = \int_{\lambda} I(\lambda) \bar{y}(\lambda) d\lambda. \tag{11}$$

The CIE XYZ colour space is chosen because the Y channel is representative of the M cone's spectral sensitivity for photopic vision; and thus, describes the luminance of the scene. The X channel contains a combination of the three CIE RGB curves, and the Z channel is related to the blue channel in RGB. Therefore, at a given Y value, the XY plane contains all chromaticities at that luminance. Moreover, the luminance is related to gloss as it can be defined as the sum of the distributions of the volume diffusion and the surface reflection caused by the microfacets [16].

These values are used to fit and optimise the parameters k_s, R_d, and α_g into the BRDF model. Using a genetic algorithm [49–51], the cube root cosine weighted root mean squared (RMS) formula is used as an objective function, defined as:

$$ost = \sqrt{\frac{\Sigma((M(\theta_i, \theta_r) \cos\theta_i - E(\theta_i, \theta_r, p) \cos\theta_i)^2)^{1/3}}{n}}, \tag{12}$$

where M are the measured CIE XYZ values (Eq. 10) and E are the estimated BRDF values obtained using the Cook-Torrance GGX BRDF model (Eq. 9), with the parameters p, calculated for the n pairs of incident and reflected directions. The minimum and maximum values for the BRDF coefficients to be optimised and the initial parameters used in the genetic algorithm optimisation problem are presented in Tables 2 and 3, respectively. Each CIE XYZ channel is optimised individually, giving a set of three models per surface. The cube root cosine weighted RMS function is used because the cosine weight compensates for the reflectance increase towards grazing angles and the cube root compressive metric is used to avoid overemphasising the importance of BRDF peaks in the mirror angle [52].

Table 2 Minimum and maximum values for the BRDF coefficients to be optimised

	α	k_s	R_d
Min	0.05	0.01	0
Max	0.99	0.5	5

Perceptual dimensions of gloss

Gloss is a function of a surface's directional reflectance. Hunter defines at least six visual phenomena related to apparent gloss [53]. In this paper, focus is given to contrast gloss and distinctness of image (DOI) gloss as they have been defined as perceptual dimensions of glossy appearance [54].

Contrast gloss is defined as the perceived relative brightness of specularly and diffusely reflecting areas, defined by Ferwerda et al. [54], and given by:

$$c = \sqrt[3]{k_s + \frac{R_d}{2}} - \sqrt[3]{\frac{R_d}{2}}, \tag{13}$$

where k_s is the specular weighted parameter and R_d is the diffuse component of the BRDF (Eq. 7). DOI gloss is defined as the perceived sharpness of images reflected in a surface and is given by:

$$d = 1 - \alpha, \tag{14}$$

where α is the width parameter for the specular lobe used to model the specular component, R_s (Eq. 15).

Multivariate analysis

Multivariate analysis provides a statistical evaluation of various simultaneous observations. In this

Table 3 Initial parameters used for the optimisation problem

Max iterations	# population	Beta	pC	Gamma	Mu	Sigma
100	1000	1	1	0.01	0.05	0.01

subsection, multivariate methods used in this paper will be presented.

Principal component analysis

Principal component analysis (PCA) [55, 56] is a popular method of dimensionality reduction. PCA looks for a projection which transforms the data into a new coordinate space where most of the variation in the data can be described in fewer dimensions than the original data. Here, PCA is applied to the fitting parameters, α, k_s, and R_d, obtained to model the BRDF of the surfaces, and to the gloss attributes, c and d, using 5 principal components (PCs). The data is preprocessed by performing scaling and centring.

Mahalanobis distance metric

The Mahalanobis distance is a measure of distance between a point, P, and a distribution, D. When P is at the mean of D, the distance is zero, and increases as P moves away from the mean along each principal component axis [57]. The Mahalanobis distance is favoured since it is unitless, scale-invariant and takes into account the correlations of the dataset.

Results and discussion

In this section, conventional colour and gloss results, widely used in restoration-conservation studies, are presented. Then, appearance classification results obtained

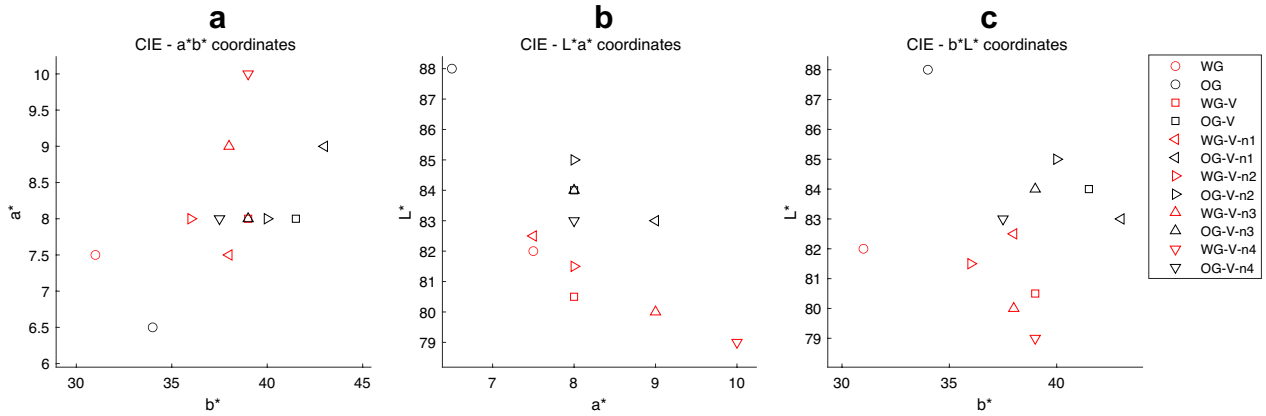

Fig. 7 Average L*, a*, b* values for oil gilding (black) and water gilding (red), unvarnished (round marker), varnished (square marker), n1 (left pointing marker), n2 (right pointing marker), n3 (top pointing marker), and n4 (bottom pointing marker). **a** CIE a*b* coordinates. **b** CIE L*a* coordinates. **c** CIE L*b* coordinates

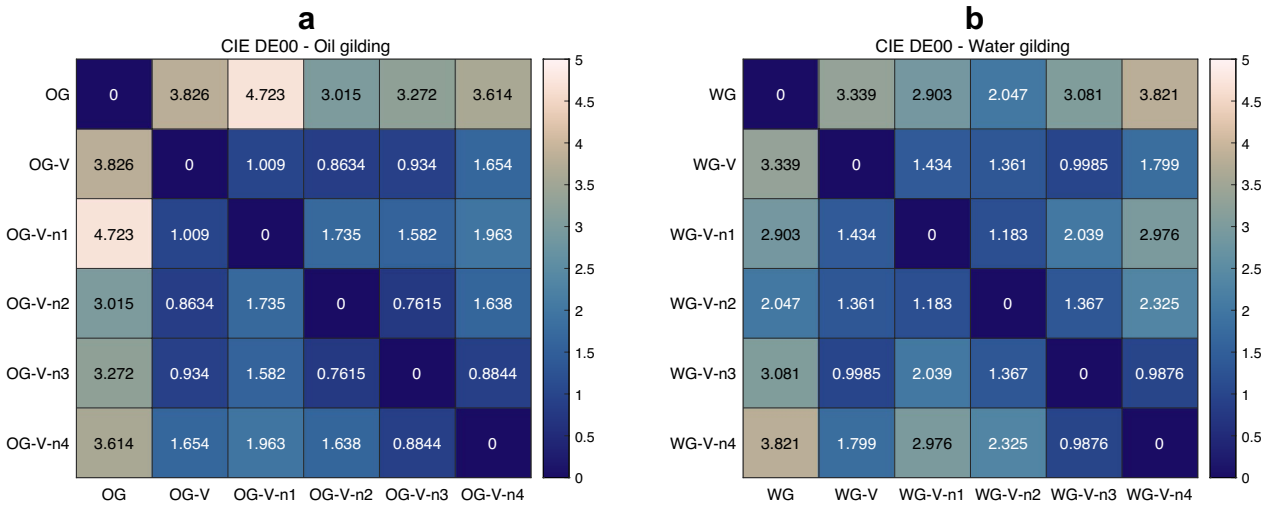

Fig. 8 CIE DE00 values calculated for **a** oil gilding and **b** water gilding. Values lower than 1 are below the JND

from bidirectional reflectance measurements are discussed as an alternative to the former.

Conventional colour and gloss measurements

Colour was measured following the method presented in *Conventional colour and gloss measurements* and the average CIE L*a*b* coordinates are calculated using CIE standard illuminant D65 and CIE 10° standard observer colour matching functions (Fig. 7). The colour difference between all the samples was calculated using CIE ΔE 2000 (DE00) colour difference formula (Fig. 8), where values lower than 1 are below the just noticeable difference (JND).

Two clusters can be identified, water gilding samples have higher L* values than oil gilding (Fig. 7). Varnishing is expected to saturate both types of gilding, L* decreases and b* increases, producing a perceptible colour change as the luminance decreases and the chroma shifts to higher values of b* (Fig. 8).

Each varnish removal method changes the colour of the gilded surfaces differently. In the case of oil gilding, the colour difference between the four cleaned samples and OG-V is lower than the JND in the case of n2 and n3, suggesting an unperceivable colour difference, and just above the JND for n1 and n4 (Fig. 8). All varnish removal methods reduce the colour difference between the surface and the unvarnished reference, except for n1. For water gilding, the colour difference between the cleaned surfaces and the varnished surface is just above the JND for all methods except n3 (Fig. 8). Like oil gilding, removing the varnish reduces the colour difference between them and the reference, with exception of n4. In general, removing varnish from gilded surfaces has a more significant effect on water gilding than oil gilding.

Gloss was measured three times for each surface at 20°, 60°, and 85° and the results were averaged for each measurement angle (Fig. 9). For oil gilding, at 20°, the reference sample has the highest gloss. The varnished and cleaned surfaces have a similar gloss. At 60°, the varnished surface has lower gloss than the reference but, n2 has a slightly higher gloss than the reference. At 85°, the varnished surface has the highest gloss, n1 and the reference have similar values of gloss. The other three cleaning methods have lower gloss values than the reference.

In the case of water gilding, the relative differences in gloss are similar at the three measurement angles. In general, the unvarnished sample has the highest gloss. Varnishing decreases the gloss by almost two orders of magnitude in the case of 20° and 60°, and by a factor of 5 at 85°. Cleaning the varnish increases the gloss at all angles. Method n3 has the highest effect, at 20° and at 60°, n1, n2, and n4 are very similar. At 85°, n1 has gloss values closer to n3, then n2 and finally n4.

The glossmeter measurements show that varnishing decreases the gloss of the gilded samples, except for oil gilding at 85°. In the case of water gilding, the effect of varnishing decreases the gloss almost by a factor of 7 for all measurement angles. These results contradict empirical knowledge which states that varnishing increases the gloss of surfaces. It must be emphasised that gloss measurements are not easily correlated to human perception; and thus, when evaluating appearance changes caused by conservation methods, traditional gloss measurements must be interpreted with caution.

Conventional colour and gloss measurements are insufficient to fully understand appearance changes in gilded surfaces caused by varnishing. Colour measurements

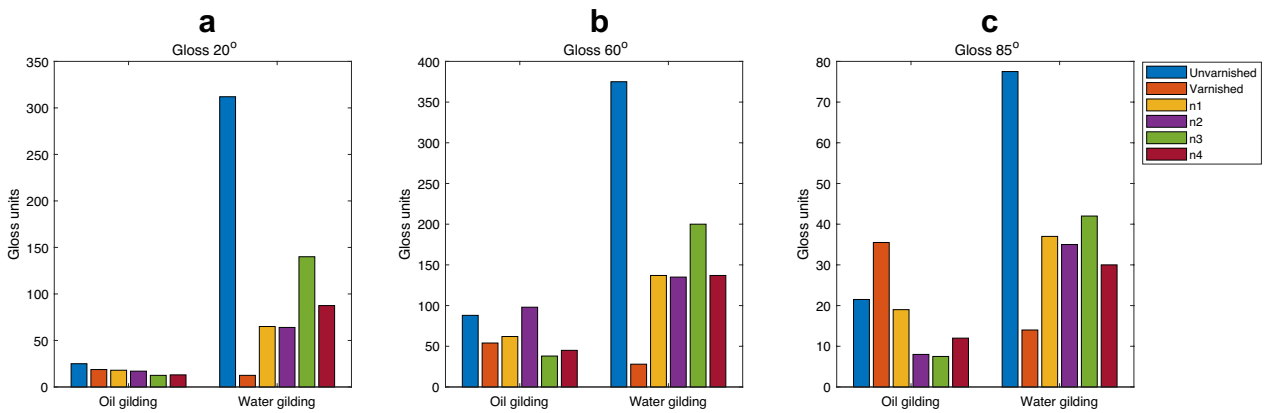

Fig. 9 Average gloss at **a** 20°, **b** 60°, and **c** 85°. Values for oil gilding (left) and water gilding (right), unvarnished (blue), varnished (orange), n1 (yellow), n2 (purple), n3 (green), and n4 (maroon)

provide a starting point in characterising the effects of varnishing and removing varnish. Yet, the colour differences calculated here are not correlated to perception. While some surfaces have colour differences of less than a JND, a clear difference in appearance is perceived by visual inspection. Gloss measurements are harder to interpret as gloss units are not easily correlated to perception. Moreover, the gloss measurements obtained above contradict empirical knowledge and experience. An evaluation of cleaning methods based on gloss measurements is not possible as the results oppose visual perception. Therefore, the appearance of gilded surfaces must be measured using alternative methods to have a better understanding of how it is affected by varnishing and the removal of varnish.

Bidirectional reflectance measurements

In this subsection, the results obtained with the bidirectional imaging system are presented. The samples were measured following the methodology proposed in *Flexible HDR multispectral-imaging BRDF system,*, and the data was processed accordingly, to obtain CIE 1931 XYZ values as a function of the angle of incidence, θ_i, for the fixed angle of reflection, $\theta_r = -22.5°$. The data is modelled to the Cook-Torrance BRDF model and GGX distribution, using a genetic algorithm.

The BRDF parameters estimated for each surface at each CIE XYZ channel and the minimum error obtained are presented in Table 4. The mean and maximum error values achieved were 0.178 and 0.262 respectively. These values are within the acceptable quality range; thus, the models represent well the measured data.

The BRDF coefficients are used to model the BRDF of the surface at the fixed angle of viewing, $\theta_r = -22.5°$, as a function of the angle of illumination, θ_i (Fig. 10). The left column shows the BRDF obtained for oil gilding, and the right column shows the BRDF obtained for water gilding.

For all the samples, the coefficients fitted for CIE Z are different from those fitted for CIE X and Y (Table 4). This implies that the goniochromatism in the CIE X and Y channels has a similar BRDF, but the BRDF in the CIE Z channel is different. The CIE Z channel is representative of the blue channel in the RGB space, which could explain this difference. The polar plots (Fig. 10) show similar specular lobes for CIE X and Y, but different for CIE Z, in the case of both types of gilding. In the

Table 4 BRDF model estimated coefficients and cosine cubic weighted RMS cost obtained using a genetic algorithm

	Oil gilding				Water gilding			
	α	k_s	R_d	cost	α	k_s	R_d	cost
Unvarnished								
CIE X	0.651	0.074	4.915	0.262	0.897	0.062	0.923	0.245
CIE Y	0.650	0.077	5.000	0.260	0.852	0.067	0.753	0.240
CIE Z	0.808	0.122	1.234	0.175	0.490	0.052	0.124	0.250
Varnished								
CIE X	0.343	0.060	2.218	0.193	0.462	0.052	1.751	0.175
CIE Y	0.371	0.066	2.130	0.190	0.480	0.057	1.584	0.173
CIE Z	0.222	0.054	0.471	0.183	0.192	0.037	0.430	0.166
n1								
CIE X	0.729	0.110	4.815	0.185	0.659	0.083	4.785	0.226
CIE Y	0.768	0.116	5.000	0.180	0.688	0.089	4.923	0.219
CIE Z	0.518	0.152	0.268	0.147	0.489	0.110	0.534	0.169
n2								
CIE X	0.724	0.128	4.382	0.158	0.728	0.082	4.755	0.192
CIE Y	0.770	0.134	4.831	0.155	0.759	0.088	4.916	0.190
CIE Z	0.497	0.161	0.427	0.142	0.451	0.091	0.560	0.148
n3								
CIE X	0.865	0.177	4.131	0.129	0.781	0.094	4.261	0.155
CIE Y	0.873	0.181	4.019	0.128	0.817	0.099	4.400	0.150
CIE Z	0.542	0.215	0.134	0.124	0.250	0.082	0.598	0.152
n4								
CIE X	0.764	0.112	4.889	0.170	0.826	0.075	4.380	0.200
CIE Y	0.776	0.115	4.838	0.170	0.859	0.082	4.312	0.183
CIE Z	0.472	0.134	0.383	0.147	0.243	0.058	0.516	0.198

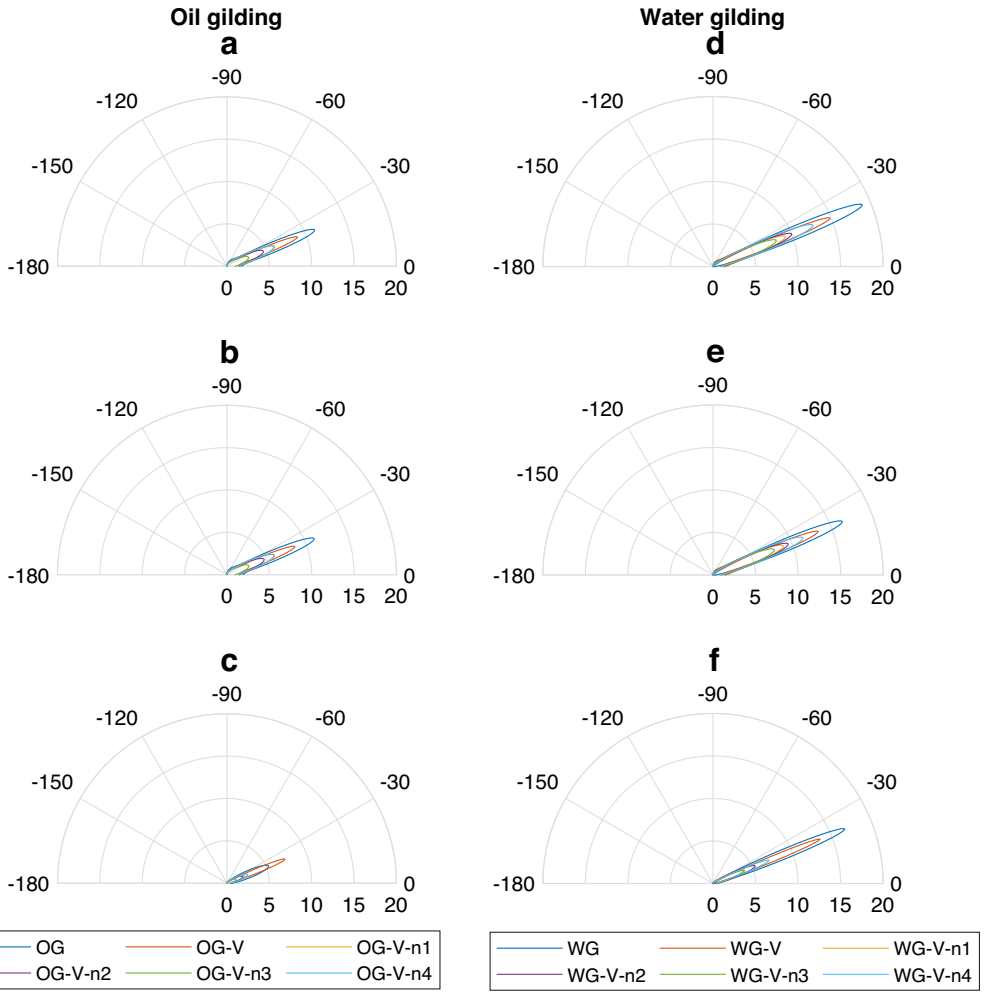

Fig. 10 Polar plot of modelled CIE XYZ values of each surface as a function of illumination angle, at fixed angle of viewing, $\theta_r = -22.5°$. Oil gilding **a**: CIE X, **b**: CIE Y, **c**: CIE Z. Water gilding **d**: CIE X, **e**: CIE Y, **f**: CIE Z

case of oil gilding, the varnished sample has the highest magnitude in the Z coordinate.

The specular lobe of the three CIE XYZ coordinates for the oil gilding samples is smaller than that of the water gilding samples, suggesting water gilding is glossier than oil gilding. This is also suggested by the values of k_s which in general are lower for water gilding than oil gilding (Table 4).

The BRDF coefficients are used to render the Adobe RGB visualisation of the surfaces at angle of viewing $\theta_r = -22.5°$, and angles of illumination ranging from $-57°$ to $12°$. (Fig. 11). The left column displays the visualisations of the oil gilding samples, and the column on the right shows the water gilding samples. The order from top to bottom is reference, varnished, n1, n2, n3, and n4.

The appearance of the Adobe RGB rendered images of the modelled BRDF is representative of the visual appearance of the varnished gilded surfaces (Fig. 11), these visualisations provide supplementary visual information which discriminates an oil-based gilded surface, from a water-based gilded surface, and indicates the presence (or not) of a varnish layer on the gold leaf. Moreover, in the context of varnish removal, the images allow to visualise the impact of the different treatments on a gilded surface, and to classify the types of gilding and to discriminate their characteristics. The visualisations allow to discriminate the various levels of gloss of the different surfaces and are similar to the gilded surfaces of the mock-ups. These nuances give a visual scale, which allows, in this case, to control the varnish removal and define the limits of acceptability.

Perceptual gloss attributes

The BRDF coefficients obtained for the CIE Y channel, representative of luminance, are used to calculate

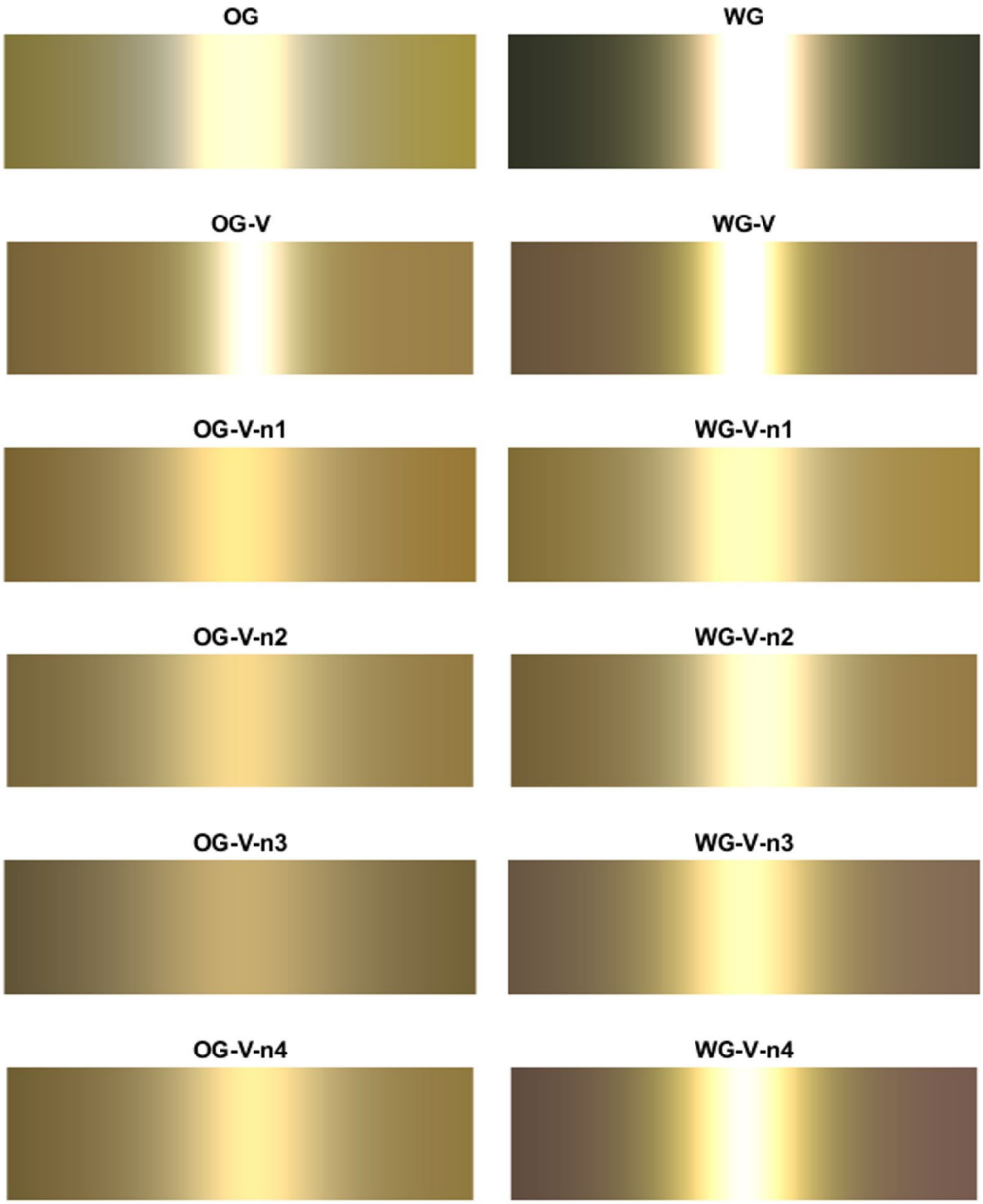

Fig. 11 Adobe RGB rendered images of the modelled BRDF of each surface at fixed viewing angle, $\theta_r = -22.5°$. Each 10 pixels on the horizontal axis represent a step of one degree in angle of incidence

contrast gloss, *c*, and DOI gloss, *d*, values according to Eq. 13 and Eq. 14 respectively. (Fig. 12). The CIE Y channel is chosen since the luminance is correlated to the gloss BRDF [16].

Varnishing increases the contrast gloss, *c*, for both gilding techniques. The four varnish removal methods decrease *c* compared to the varnished area. In the case of oil gilding, n1 and n4 have the weakest effect on *c*, and n2 decreases the value of *c* the most. For water gilding, the varnish removal methods have a value of *c* from higher to lower in the order n1, n2, n3, and n4.

Unvarnished water gilding has a value of DOI gloss, *d*, 8 times higher than unvarnished oil gilding. The DOI gloss, *d*, is also affected by varnishing. The two varnished samples, oil and water gilding, have the same value of *d*. In the case of oil gilding, *d* increases by a factor of 4. While for water gilding, varnishing decreases the value of *d* by half. Varnish removal methods n1, n2, and n4 decrease

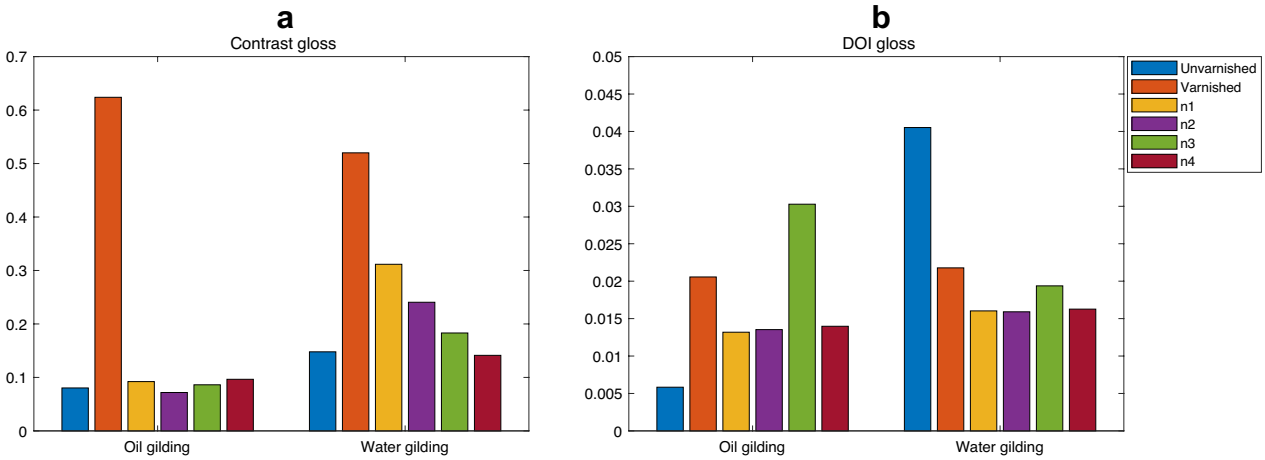

Fig. 12 **a** Contrast and **b**DOI gloss values obtained from BRDF coefficients modelled for oil gilding (left) and water gilding (right) for unvarnished (blue), varnished (orange), n1 (yellow), n2 (purple), n3 (green), and n4 (maroon)

the value of *d* by the same amount for both types of gilding. In the case of oil gilding, n3 increases the value of *d*.

These results are consistent with visual perception and empirical knowledge, and can be explained by the translucent nature of varnish. Varnishing the surface implies adding an interface in the stratigraphy of the gilding. Gold has a very high extinction index ($0.37 + 2.82i$ at 600 nm [58]), making it very opaque and reflecting. Varnish, on the other hand, is a refractive medium. In the case of unvarnished oil gilding, both contrast gloss and DOI gloss are lower than that of water gilding. This is expected since both surfaces have very different roughness; being smoother water gilding is glossier. However, once varnished, both oil and water gilded surfaces are very similar in appearance. The varnish has a saturating effect which is reflected in an increase in contrast gloss for both types of gilding. It also increases the DOI gloss of oil gilded surfaces; however, it has the opposite effect on water gilding. The varnish smooths the surface roughness of oil gilding, increasing its DOI gloss. In the case of water gilding, varnishing decreases the DOI gloss because the varnish acts as an interface where refraction and scattering decrease the perceived sharpness of the reflected image. The effect of refraction and scattering of varnish on oil gilding is lower than the effect of its surface roughness. However, for water gilding, the opposite is true since its original surface is smoother.

The contrast and DOI gloss values, unlike traditional gloss measurements, are consistent with the visual perception of the gilded surfaces as well as empirical knowledge and experience of conservators. These results suggest that varnishing gilded surfaces increases both contrast and DOI gloss in the case of oil gilding, and only contrast gloss in the case of water gilding; which is expressed as a general increase in gloss by conservators.

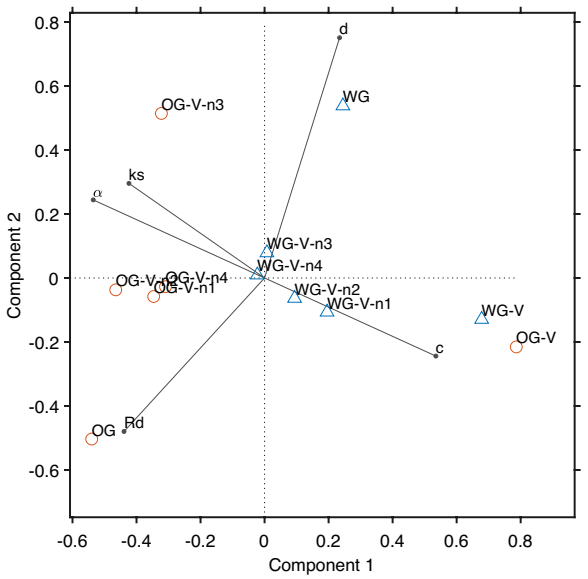

Fig. 13 Biplot of the PCA for the first two PCs, calculated using the coefficients obtained for the BRDF model in the CIE Y coordinates (α, k_s, and R_d) and gloss attributes (*c* and *d*). Oil gilding samples are displayed in orange (round markers), and water gilding samples are displayed in blue (triangle markers). PC1 and PC2 are representative of *c* and *d* respectively. Surfaces are clustered depending on their varnish level (reference or no varnish, varnished, and cleaned)

Clustering based on perceptual gloss attributes

The BRDF coefficients obtained for all the samples at the CIE Y channel, as well as the corresponding c and d values for the same channel are used to perform a principal component analysis (PCA) with 5 principal components (PCs), with scaling and centring of the data. The first three PCs give a cumulative explained variance of 96%.

The first two PCs can be interpreted as perceptual axes. PC1 is strongly correlated to contrast gloss, c, which by definition is inversely proportional to α. PC2 is strongly correlated to the difference between distinctiveness of image gloss, d, and R_d (Fig 13).

Based on the PCA, clear clusters are formed. Firstly, the reference surfaces are at opposite ends of the PC space. OG lies in the negative quadrant of both PC1 and PC2, whereas WG lies in the positive quadrant for both PCs. This implies that both surfaces are the most different in terms of their appearance. WG has a high DOI gloss and relatively high contrast gloss, OG has a low DOI gloss and lower contrast gloss. This confirms common knowledge that oil and water gilding have very different appearance, since water gilding is burnished, it has a glossy effect, unlike oil gilding.

The varnished samples are also clustered in one group. They have a positive PC1 value and negative PC2 value. Varnishing the samples increases the contrast for both types of gilding. However, the DOI gloss of water gilding decreases whilst for oil gilding it increases. These changes produce a similar appearance for both types of gilding when varnished, which is consistent with empirical knowledge and experience.

Finally, the cleaned surfaces are clustered in two groups, dependent on their gilding type. Oil gilding samples are on the negative scale of PC1 and near 0 for PC2. Water gilding on the other hand, are closer to the origin, in the positive scale of PC1. This implies that oil gilding samples in general have lower contrast and DOI gloss than water gilding samples. OG-V-n3 does not belong to any cluster, as it lies on the negative scale of PC1 but positive scale of PC2.

While the different varnish removal methods (except for OG-V-n3) give each type of gilding a similar appearance, none of them restore the original appearance of the gilding before varnishing, nor maintain the appearance of the originally varnished surface.

The Mahalanobis distance [57] is calculated between each surface to evaluate the varnish removal methods, using the first three PCs which have a cumulative explained variance of 96%. (Fig. 14). The varnish layer is considered a part of the stratigraphy of the artwork, thus, the most desirable method is the one which produces an appearance closest to that of the varnished sample. The varnish removal methods are ranked from closest to furthest in appearance compared to the varnished layer. For oil gilding, the method which gives the closest appearance is n2, followed by n1, n4, and finally n3. For water gilding the order is n2, n3, n4, and finally n1.

Varnish removal method n2, which produces the closest appearance to that of the original varnished surface, involves the application of the solvent by applying a compress. This method does not involve any mechanical action on the surface and does not leave residues on the

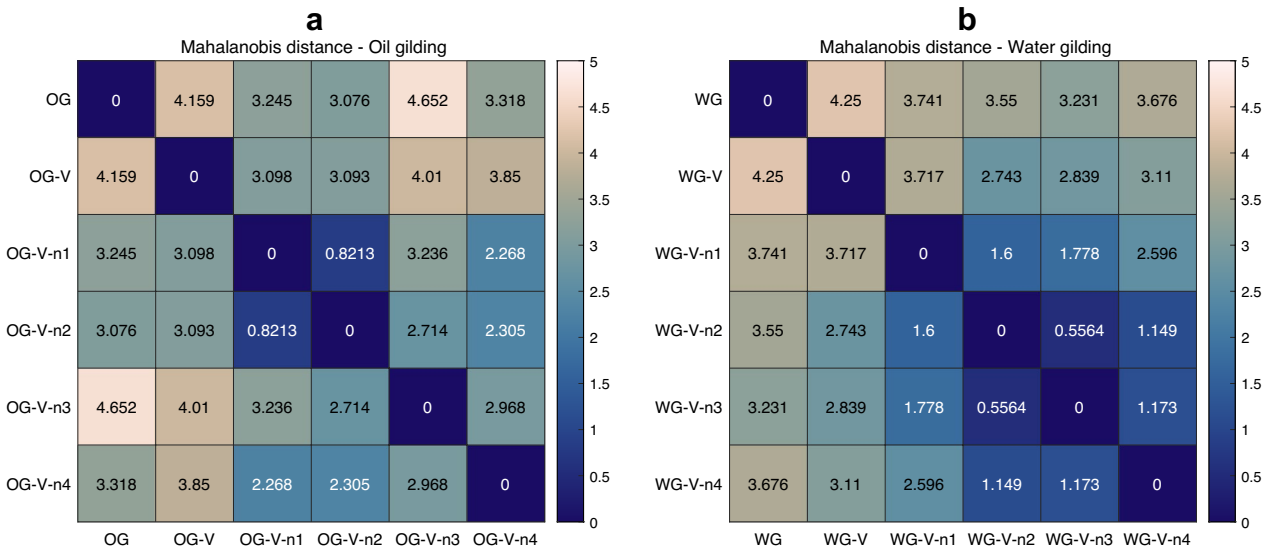

Fig. 14 Mahalanobis distance calculated between each surface in the PC space (Fig. 13) using the first three PCs for **a** oil gilding and **b** water gilding

surface, which could be the main reasons why it gives the best results. Methods n1 requires mechanical action with a cotton swab to remove the varnish which can result in abrasion of the gold leaf. Methods n3 and n4 differ in the nature of the gel used, but both methods require the solvent to be rinsed with a cotton swab which is abrasive in nature. Moreover, method n3 is a water-based gel, which due to its water content can alter water sensitive surfaces, such as oil gilding. This could explain why in the case of oil gilding, n3 causes the strongest appearance change, while in the case of water gilding it gives a satisfying result.

Visual examination by a professional conservator

A professional conservator specialised in gilded surfaces was consulted to provide a visual examination of the mock-ups and the effect the different conservation procedures have. They stated that the varnished oil gilding sample had a glossier appearance than the reference oil gilding, and an appearance closer to that of varnished water gilding which is consistent with the results presented above.

Regarding the varnish removal methods, in the case of oil gilding, method n1 produced a strong cleaning. However, there were residues of varnish on the surface distributed in a non-homogeneous way. Method n2 produced a homogeneous cleaning, leaving a thin film of varnish on the surface. Method n3 gave a very aggressive stripping of the varnish, even to the point of damaging the gold foil. This could be the reason why n3 is not clustered with the other cleaned oil gilded samples (Fig. 13). Finally, n4 produced an aggressive and non-homogeneous removal leaving some varnished as well as unvarnished areas on the sample.

For the water gilding samples, method n1 produced a non-homogeneous, slightly aggressive clearance of the varnish, most likely due to the mechanical action of the cotton bud required to remove the varnish. Method n2 gives out a homogeneous clearing of the varnish. Method n3 also generated a homogeneous clearing of the varnish with a fine layer of varnish residue. In the case of method n4, the varnish was cleaned but not completely cleared. These comments confirm the results obtained by the cluster analysis (Fig. 14). The conservator concluded that for them, the best method to remove varnish from an oil gilded surface was method n2, while for a varnished, water gilded surface methods n2 and n3 were the most appropriate.

The results obtained by measuring the BRDF of the surfaces provide additional visual information on the appearance of the metal surface (Fig. 11), as well as a quantified approach to discriminate the gloss of water gilding and oil gilding, and indicates the presence or not of surface coatings on the gilding. In addition, this analysis in the context of varnish removal, makes it possible to characterise the presence of a layer of varnish on the gold leaf, not visible to the naked eye. Therefore, the varnish removal approach can be influenced by these results and controlled quantitatively. For example, in the case of oil gilding, method n3, has damaged the gold leaf due to the aqueous nature of the gel. This can be visualised in the render of the BRDF of the surface as OG-V-n3 has a distinct visual appearance, very different from both the unvarnished and varnished visualisations.

Conservation of the *Vierge de douleur/Virgin of sorrows*

As part of the conservation work carried out at the National Heritage Institute, the *Vierge de douleur/Virgin*

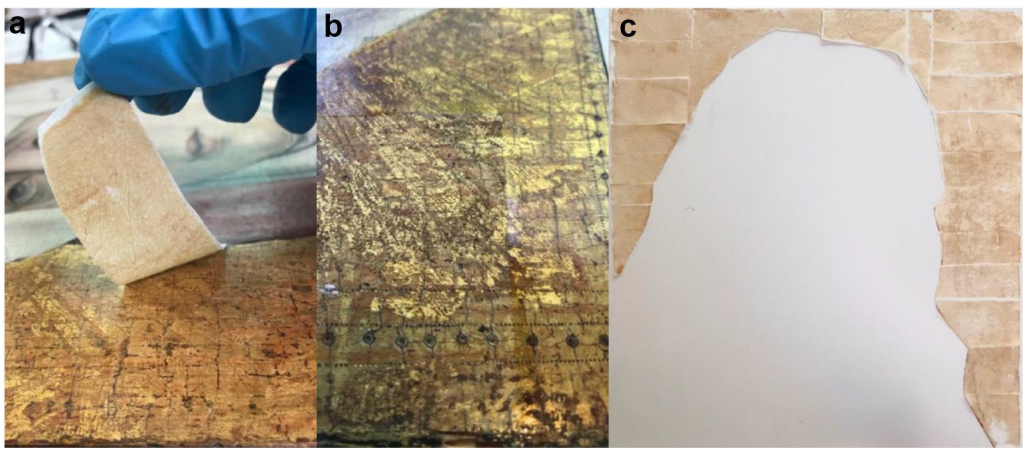

Fig. 15 Conservation of the *Vierge de douleur/Virgin of sorrows*. **a** Removal of varnish using Evolon®CR compress soaked with solvent. **b** Detail of an area of the painting after removing the varnish. **c** Entire counterform of the gilding, in Evolon®CR, after the varnish removal process

of sorrows underwent a restoration campaign. Kept in storage since its acquisition by the Jacquemart-André Museum, it was until now unknown to the public. Its study and conservation enable to re-appreciate this work, rich in values.

The conservation work consisted of a structural securing of the panel and the frame, and seeks to harmonise the appearance of the whole, mainly through a cleaning work. Targeted research on the cleaning of varnished gilding has been carried out, in order to guide the restoration treatments. Following the results presented above, as well as complementary analyses, the painting was cleaned by solubilisation by applying a compress, with particular attention against the use of cotton for this operation. (Fig. 15). Moreover, removing the varnish by applying a compress, not only produces the smallest change in gloss and causes no abrasion, but also is the most reproducible and homogeneous method, maintaining a very thin layer of varnish which is beneficial for the protection of the gilding from external degradation factors.

Conclusions and future work

This paper presents a framework for characterisation, classification, and evaluation of oil gilded and water gilded surfaces as well as the effect on appearance of varnish, and varnish removal methods.

It is shown that conventional colorimetric and gloss measurement and analysis are insufficient to properly characterise the appearance of gilded surfaces, and evaluate the appearance changes induced by different restoration processes such as varnishing and varnish removal methods.

To overcome this issue, an imaging system is used to measure the bidirectional reflectance of mock-ups of unvarnished oil gilding and water gilding, varnished mock-ups, and mock-ups cleaned with four different chemical varnish removal methods. By performing a PCA on the BRDF model coefficients as well as perceptual gloss attributes, clear groups can be identified. The evaluation of cleaning methods based on the PCA clusters are consistent with visual inspection by a professional conservator.

In particular, the results show that the varnishing effect is irreversible on the appearance of gilding. As expected, water gilding has the highest DOI gloss, and oil gilding has the lowest DOI gloss. It is found that varnishing modifies the appearance of both types of gilding, making their appearance more similar to each other. Furthermore, either for water or oil gilding, none of the varnish removal methods restore the gilding to its original appearance due to the fragility of the gold foil.

For future studies, this methodology could be applied on investigating the effects of ageing on the appearance of gilded surfaces and the effects of varnish removal methods on aged, gilded surfaces. It must be clarified that the method presented here focuses only on appearance changes induced by varnishing gilded wood, as well as effects due to varnish removal methods. A broader evaluation on cleaning methods must also consider other factors such as the uniformity of the cleaning, remnants of varnish on the surface, lacunas, stripping of the gold foil, absorption of the solvents by the surface, etc.

The methodology presented in this paper allows to not only characterise and cluster different gilded surfaces accurately, but does so in a coordinate space which is correlated to human perception, by using perceptual gloss attributes. Gloss attributes are necessary to explain the changes in appearance, whether due to different gilding techniques, varnishing, or different cleaning methods, and these are accurately represented in the component space. Moreover, this methodology can evaluate cleaning methods with results consistent to those of visual examination by experts.

Finally, a 15th-century panel painting and its 19th-century neo-gothic frame were restored, involving a cleaning campaign guided by the results obtained by this framework. Solubilisation by applying an Evolon®CR compress has proven to be an effective method which creates the minimum change in appearance, as well as being homogeneous, maintaining a thin layer of varnish which protects the gilding from external degradation factors.

Appendix

Technological study of the artwork

To guide the conservation of the painted panel a technological study was conducted to identify its materials and fabrication methods [59]. Macro XRF showed that only pure gold leaf was used in the gilding. The contracts from this time period suggest the use of a 23 karat gold leaf [60]. Water gilding would be the most appropriate technique for this type of work. However, the stratigraphic cross-section reveals the presence of an extremely thin orange layer under the gold leaf, composed of ochre. Due to the lack of lead pigments almost systematically used as driers in the mordant [60], oil gilding is dismissed as a possible fabrication technique. A third technique, less known and less documented, could have been used. It is a water-based gilding that does not use a bole, but only a charged preparation. This is bound with fish glue and egg white or honey, and coloured with cinnabar and saffron. The gold leaf is placed directly on this preparation, or dry by reapplying water [4]. It is

difficult to know whether the gold leaf was burnished or not: the absence of a bole as well as the great finesse of the gold leaf would make this process difficult [60]. Moreover, binocular microscopic observation revealed the presence of a translucent orange film over the gold, most likely a glaze applied uniformly over the gold leaf to create a "vermillonage" [4].

Gas chromatography coupled with mass spectrometry analysis of the varnish on the painted panel reveals the presence of colophony pine resin, oil, and dammar resin. While it is hypothesised that the colophony and oil found on the painting belong to the original varnish, the dammar resin must be a product of previous conservation campaigns since it was first used in Europe in 1829 [61].

Bidirectional reflectance modelling

GGX distribution Walter et al. [62] propose a Bidirectional Scattering Distribution Function (BSDF) called GGX. This GGX BRDF is inspired by the micro-facet model proposed by Cook and Torrance. The general form of the GGX is given by:

$$R_s = \frac{1}{4}\frac{FDG}{(\mathbf{n}.\mathbf{l})(\mathbf{n}.\mathbf{v})}, \tag{15}$$

The GGX normal distribution function of micro-facets is given by:

$$D = \frac{\alpha_g^2 \chi^+(\mathbf{h}.\mathbf{n})}{\pi \cos^4\theta_h(\alpha_g^2 + \tan^2\alpha_h)^2}, \tag{16}$$

where α_g is a width parameter for the specular lobe, θ_h is the angle between the half-vector, **h**, and the surface normal, **n**, and χ^+ is a positive characteristic function which equals to one if its parameter is greater than zero and zero if its parameter is lesser or equal to zero.

The geometrical attenuation factor which describes the shadowing and masking effects is derived from the GGX distribution, D (Eq. 16). This is given by the monodirectional shadowing term defined as:

$$G_1(\mathbf{v}) = \chi^+\left(\frac{\mathbf{v}.\mathbf{h}}{\mathbf{v}.\mathbf{n}}\right)\frac{2}{1+\sqrt{1+\alpha_g^2\tan^2\theta_v}}, \tag{17}$$

where θ_v is the angle between the viewing vector, **v**, and the surface normal, **n**.

Abbreviations

BRDF	Bidirectional reflectance distribution function
HDR	High-dynamic range
VIS/NIR	Visible/Near-infrared
LDR	Low-dynamic range
SCE	Specular component excluded
RMS	Root mean squared
DOI	Distinctiveness of image
PCA	Principal component analysis
PC	Principal component
DE00	ΔE 2000
JND	Just noticeable difference

Acknowledgements

The authors would like to thank Pierre Curie from the Jacquemart-André Museum who granted confidence and trust in this project, Agnès Lattuati-Derieux for her supervision in the chemical analysis, Vlado Kitanovski for his invaluable help with the data acquisition, and Doctor Malgorzata Sawicki for her revision and suggestions.

Author contributions

DM prepared the gilding mock-ups, DM and YA designed the experiments, DM and YA conducted the experiments, YA computed the results, all authors interpreted the results, YA wrote the manuscript. All authors read and approved the final manuscript.

Funding

This work has received funding from the European Union's Horizon 2020 research and innovation program under the Marie Skłodowska-Curie grant agreement No. 813789 as part of the CHANGE (Cultural Heritage Analysis for New Generations) ITN project.

Availability of data and materials

The data used and/or analysed during the current study are available from the corresponding author on reasonable request.

Declarations

Competing interests

The authors declare that they have no competing interests.

Received: 5 August 2022 Accepted: 17 January 2023
Published online: 14 February 2023

References

1. Mastrotheodoros GP, Beltsios KG, Bassiakos Y, Papadopoulou V. On the metal-leaf decorations of post-byzantine greek icons. Archaeometry. 2018;60(2):269–89. https://doi.org/10.1111/arcm.12287.
2. Sandu I, Murta E, Ferreira S, Pereira M, Kuckova S, Valbi V, Dias L, Prazeres C, Cardoso A, Mirão J. A comparative multi-technique investigation on material identification of gilding layers and the conservation state of 7 portuguese mannerist altarpieces. Int J Conserv Sci. 2015;6:439–54.
3. Sandu IA, Busani T, de Sá MH. The surface behavior of gilding layer imitations on polychrome artefacts of cultural heritage. Surf Interface Anal. 2011;43(8):1171–81.
4. Neven S. The Strasbourg Manuscript: A Mediaeval Tradition of Artists' Recipe Collections (1400–1570). London: Archetype Publication; 2016.
5. Kollandsrud K, Plahter U. Twelfth and early thirteenth century polychromy at the northernmost edge of europe: past analyses and future research. Medievalista. 2019. https://doi.org/10.4000/medievalista.2303.
6. Chaban A, Lanterna G, Gigli MC, Becucci M, Fontana R, Striova J. Multi-analytical approach to the study of mecca gilding technique. Microchem J. 2021;168: 106415.
7. Todd JT, Norman JF. The visual perception of metal. J Vision. 2018;18(3):9. https://doi.org/10.1167/18.3.9.
8. Vernardakis TG. Pigment Handbook, Vol. I, Properties and Economics. 2nd ed. New York: Wiley; 1988.
9. Saris H, Gottenbos R, Van Houwelingen H. Correlation between visual and instrumental colour differences of metallic paint films. Color Res Appl. 1990;15(4):200–5.

10. Billmeyer FW, Davidson JG. Color and appearance of metallized paint films. I. Characterization. J Paint Technol. 1974;46(593):31–7.
11. Baba, G., Arai, H.: Gonio-spectrophotometry of metal-flake and pearl-mica pigmented paint surfaces. In: 4th Oxford Conference on Spectroscopy (2003), vol. 4826, pp. 79–86. SPIE
12. Wills J, Agarwal S, Kriegman D, Belongie S. Toward a perceptual space for gloss. ACM Trans graph (TOG). 2009;28(4):1–15.
13. Obein G, Knoblauch K, Viéot F. Difference scaling of gloss: Nonlinearity, binocularity, and constancy. J vision. 2004;4(9):4.
14. Rhopoint Instruments: Appearance Measurement (2022). https://www.rhopointinstruments.com/faqs/appearance-measurement/ Accessed 18 July 2022
15. Wu Q, Hauldenschild M, Rösner B, Lombardo T, Schmidt-Ott K, Watts B, Nolting F, Ganz D. Does substrate colour affect the visual appearance of gilded medieval sculptures? Part I: colorimetry and interferometric microscopy of gilded models. Herit Sci. 2020; 8:118. https://doi.org/10.1186/s40494-020-00463-3.
16. Obein, G., Leroux, T., Vienot, F. 2001. Bidirectional reflectance distribution factor and gloss scales. In: Human Vision and Electronic Imaging VI. 2001. vol. 4299, pp. 279–290. SPIE. https://doi.org/10.1117/12.429491
17. Courtier S, Dubost M. L'or et la manière : les techniques de la dorure sur bois à travers le temps. In: Mailho L, de Reyer D, Catillon R, Leroux L, Bruhiere N, Bourges A, Cabillic I, editors. Coré - Conservation Restauration du Patrimoine Culturel. 1st ed. France: SFIIC; 2021. p. 10–29.
18. Learner, T.J., Smithen, P., Krueger, J.W., Schilling, M.R.: Modern Paints Uncovered: Proceedings from the Modern Paints Uncovered Symposium. The Getty Conservation Institute, Los Angeles. 2007. http://hdl.handle.net/10020/gci_pubs/paints_uncovered
19. Wolbers RC, Stavroudis C, Cushman M. Aqueous methods for the cleaning of paintings. In: Stoner JH, Rushfield R, editors. Conservation of Easel Paintings. 2nd ed. London: Routledge; 2020. p. 526–48.
20. Mecklenburg, M.F., Charola, A.E., Koestler, R.J.: New Insights Into the Cleaning of Paintings: Proceedings from the Cleaning 2010 International Conference, Universidad Politécnica de Valencia and Museum Conservation Institute. Smithsonian Institution Scholarly Press, Washington DC. 2013. https://doi.org/10.5479/si.19492359.3.1
21. Sawicki M, Bramwell-Davis V, Dabrowa B. Laser cleaning from a practical perspective: Cleaning tests of varied gilded-wood surfaces using Nd: YAG Compact Phoenix laser system. AICCM Bull. 2011;32(1):44–53.
22. Boonrat P, Dickinson M, Cooper M. Initial investigation into the effect of varying parameters in using an Er: YAG laser for the removal of brass-based overpaint from an oil-gilded frame. J Inst Conserv. 2020;43(1):94–106.
23. Sawicki M, Rouse E, Bianco SL, Kautto S. An investigation of the feasibility of the use of gels and emulsions in cleaning of gilded wooden surfaces. Part A: removal of brass-based overpainting. In: Nevin A, Sawicki M, editors. Heritage Wood. 1st ed. Cham: Springer; 2019. p. 1–36.
24. Sawicki M, Rouse E, Bianco SL, Kautto S. An investigation of the feasibility of the use of gels and emulsions in cleaning of gilded wooden surfaces. part b: cleaning of soiled oil-gilding. In: Nevin A, Sawicki M, editors. Heritage Wood. 1st ed. Cham: Springer; 2019. p. 37–64.
25. Albano M, Grassi S, Fiocco G, Invernizzi C, Rovetta T, Licchelli M, Marotti R, Merlo C, Comelli D, Malagodi M. A Preliminary Spectroscopic approach to evaluate the effectiveness of water-and silicone-based cleaning methods on historical varnished brass. Appl Sci. 2020;10(11):3982. https://doi.org/10.3390/app10113982.
26. Auffret, S., Nikolaus, S.B.: Cleaning of Wooden Gilded Surfaces: An Experts Meeting Organized by the Getty Conservation Institute, March 12-14, 2018. The Getty Conservation Institute, Los Angeles. 2019. http://hdl.handle.net/10020/gci_pubs/gilded_surfaces
27. Stulik D, Miller D, Khanjian H, Carlson J, Khandekar N, Wolbers R, Petersen WC. Solvent Gels for the Cleaning of Works of Art: the Residue Question. Los Angeles: The Getty Conservation Institute; 2004.
28. Darque-Ceretti E, Felder E, Aucouturier M. Foil and leaf gilding on cultural artifacts: forming and adhesion. Matéria (Rio de Janeiro). 2011;16:540–59. https://doi.org/10.1590/S1517-70762011000100002.
29. Toque, J.A., Komori, M., Murayama, Y., Ide-Ektessabi, A.: Analytical Imaging of Traditional Japanese Paintings Using Multispectral Images. In: Ranchordas, A. (ed.) VISIGRAPP: International Joint Conference on Computer Vision, Imaging and Computer Graphics Theory and Applications. 2010. pp. 119–132
30. MacDonald LW, Vitorino T, Picollo M, Pillay R, Obarzanowski M, Sobczyk J, Nascimento S, Linhares J. Assessment of multispectral and hyperspectral imaging systems for digitisation of a Russian icon. Herit Sci. 2017;5:41. https://doi.org/10.1186/s40494-017-0154-1.
31. Martinez MA, Valero EM, Nieves JL, Blanc R, Manzano E, Vilchez JL. Multifocus HDR VIS/NIR hyperspectral imaging and its application to works of art. Optics Express. 2019;27(8):11323–38. https://doi.org/10.1364/OE.27.011323.
32. Dumazet, S., Genty, A., Zymla, A., De Contencin, F., Texier, A., Ruscassier, N., Bonnet, B., Callet, P.: Influence of the substrate colour on the visual appearance of gilded sculptures. In: Georgopoulos, A. (ed.) XXI International CIPA Symposium. 2007. pp. 01–06
33. Mounier A, Daniel F. The role of the under-layer in the coloured perception of gildings in medieval mural paintings. Open J Archaeom. 2013;1(1):16. https://doi.org/10.4081/arc.2013.e16.
34. Sidorov, O., Hardeberg, J.Y., George, S., Harvey, J.S., Smithson, H.E.: Changes in the Visual Appearance of Polychrome Wood Caused by (Accelerated) Aging. In: Hebert, M. (ed.) Proceedings of the IS &T International Symposium on Electronic Imaging: Material Appearance. 2021. vol. 32, pp. 1–8. Society for Imaging Science and Technology. https://doi.org/10.2352/ISSN.2470-1173.2020.5.MAAP-060
35. Arteaga, Y., Sole, A., Hardeberg, J.Y., Boust, C.: Characterising appearance of gold foils and gilding in conservation and restoration. In: Sole, A., Guarnera, D. (eds.) Proceedings of the 11th Colour and Visual Computing Symposium, Gjøvik. 2022
36. Feller, R.L.: The relative solvent power needed to remove various aged solvent-type coatings. In: Congress of the International Institute for the Conservation of Historic and Artistic Works, Lisbon. 1972
37. Baij L, Astefanei A, Hermans J, Brinkhuis F, Groenewegen H, Chassouant L, Johansson S, Corthals G, Tokarski C, Iedema P.Solvent-mediated extraction of fatty acids in bilayer oil paint models: a comparative analysis of solvent application methods. HeritSci. 2019;7:31.
38. Baij L, Liu C, Buijs J, Alvarez Martin A, Westert D, Raven L, Geels N, Noble P, Sprakel J, Keune K. Understanding and optimizing Evolon® CR for varnish removal from oil paintings. Herit Sci. 2021;9:155.
39. Tauber G, Smelt S, Noble P, Kirsch K, Siejek A, Keune K, van Keulen H, Smulders-De Jong S, Erdman R. Evolon CR: Its use from a scientific and practical conservation perspective. AIC Paintings Specialty Group Postprints. 2018;31:45–50.
40. Arteaga, Y., Hardeberg, J.Y., Boust, C.: HDR multispectral imaging-based BRDF measurement using flexible robot arm system. In: Proceedings of the 30th Color and Imaging Conference, Scottsdale. Society for Imaging Science and Technology. 2022.
41. x-Rite: ColorChecker white balance (2022). https://www.xrite.com/en/categories/calibration-profiling/colorchecker-white-balance Accessed 18 Oct 2022
42. Image Science Associates: ColorGauge Nano Target (2022). https://www.imagescienceassociates.com/colorgauge-nano-target.html. Accessed 18 Oct 2022
43. Eschbach, R., Brauers, J., Marcu, G.G., Schulte, N., Bell, A.A., Tominaga, S., Aach, T. Multispectral high dynamic range imaging. In: Color Imaging XIII: Processing, Hardcopy, and Applications. SPIE, 2008. pp. 26–37. https://doi.org/10.1117/12.761105
44. Nicodemus, F.E., Richmond, J.C.: Geometrical considerations and nomenclature for reflectance. National Bureau of Standards. 1977
45. Cook RL, Torrance KE. A reflectance model for computer graphics. ACM Transactions Graph. 1982;1(1):7–24.
46. Sole A, Farup I, Nussbaum P, Tominaga S. Bidirectional reflectance measurement and reflection model fitting of complex materials using an image-based measurement setup. J Imaging. 2018;4(11):136. https://doi.org/10.3390/jimaging4110136.
47. Sole A, Guarnera GC, Farup I, Nussbaum P. Measurement and rendering of complex non-diffuse and goniochromatic packaging materials. Visual Comput. 2021;37(8):2207–20.
48. Torrance KE, Sparrow EM. Theory for off-specular reflection from roughened surfaces. J Opt Soc Am. 1967;57(9):1105–12.
49. Bremermann HJ. The Evolution of Intelligence: The Nervous System as a Model of Its Environment. Department of Mathematics. Seattle: University of Washington; 1958.

50. Fraser AS. Simulation of genetic systems by automatic digital computers II Effects of linkage on rates of advance under selection. Aust J Biol Sci. 1957;10(4):492–500.
51. Holland JH. Adaptation in Natural and Artificial Systems: an Introductory Analysis with Applications to Biology, Control, and Artificial Intelligence. Massachusetts: MIT press; 1992.
52. Fores, A., Ferwerda, J., Gu, J. Toward a perceptually based metric for BRDF modeling. In: 20th Color and Imaging Conference, vol. 2012, pp. 142–148. Society for Imaging Science and Technology
53. Hunter RS. Gloss investigations using reflected images of a target pattern. J Opt Soc Am. 1936;26(4):190–6.
54. Ferwerda, J.A., Pellacini, F., Greenberg, D.P. Psychophysically based model of surface gloss perception. In: Human Vision and Electronic Imaging VI, (8 June 2001). 4299: 291–301. SPIE. doi: https://doi.org/10.1117/12.429501
55. Jolliffe IT, Cadima J. Principal component analysis: a review and recent developments. Philos Trans R Soc A. 2016;374(2065):1–16.
56. Jackson JE. A User's Guide to Principal Components. New York: Wiley; 2005.
57. Mahalanobis, P.C.: On the generalized distance in statistics. In: Proceedings of the National Institute of Science of India. 1936. vol. 2, pp. 49–55
58. Palik ED. Handbook of Optical Constants of Solids. Boston: Academic Press; 1985.
59. Marchioni, D.: Conservation-restauration d'une vierge de douleur, panneau peint et doré de la fin du XVeme siecle, et de son cadre doré et polychromé (Musée Jacquemart-André, Paris). Recherche de provenance et datation de l'oeuvre. Étude comparative de différentes méthodes de nettoyage d'une dorure sur bois vernie. Master thesis, National Heritage Institute, Conservation Department. Paris, France. 2021
60. Kroustallis S, Gomez Gonzalez M, Miquel Juan M, Bruquetas Galan R, Perez Monzon O. Gilding in Spanish panel painting from the fifteenth and early sixteenth centuries. J Mediev Iberian Stud. 2016;8(2):313–43.
61. Fisher, S.L. Introduction to the Painting Conservation Catalogue. Introduction to Volume I: Varnishes and Surface Coatings. Washington DC: American Institute for Conservation; 1997.
62. Walter, B., Marschner, S.R., Li, H., Torrance, K.E. Microfacet models for refraction through rough surfaces. In: Eurographics Conference on Rendering Techniques. 2007, pp. 195–206. Eurographics Association

Publisher's Note